Article

Magnetic Anisotropy Tailoring by *5d*-Doping in (Fe,Co)$_5$SiB$_2$ Alloys

Diana Benea

Faculty of Physics, Babes-Bolyai University Cluj-Napoca, Kogalniceanu 1 Str., 400084 Cluj-Napoca, Romania; diana.benea@ubbcluj.ro

Abstract: Band-structure calculations were performed using the spin-polarized relativistic Korringa–Kohn–Rostoker (SPR-KKR) band-structure method, determining intrinsic magnetic properties, such as magnetic moments, magnetocrystalline anisotropy energy (MAE), and Curie temperatures, of Fe$_{5-x-y}$Co$_x$M$_y$SiB$_2$ (M = Re, W) alloys. The general gradient approximation (GGA) for the exchange–correlation potential and the atomic sphere approximation (ASA) were used in the calculations. Previous studies have shown that for Fe$_5$SiB$_2$, the easy magnetization direction is in-plane, but it turns axial for Co-doping in the range $1 < x \leq 2.5$ (y = 0). Furthermore, studies have shown that *5d*-doping enhances the MAE by enabling the strong spin–orbit coupling of Fe–*3d* and M–*5d* states. The aim of the present theoretical calculations was to find the dependence of the anisotropy constant K_1 for combined Co- and M-doping, building a two-dimensional (2D) map of K_1 for $0 \leq x \leq 2$ and $0 \leq y \leq 1$. Similar theoretical 2D maps for magnetization and Curie temperature vs. Co and M content (M = W and Re) were built, allowing for the selection of alloy compositions with enhanced values of uniaxial anisotropy, magnetization, and Curie temperature. The magnetic properties of the Fe$_{4.1}$W$_{0.9}$SiB$_2$ alloy that meet the selection criteria for axial anisotropy $K_1 > 0.2$ meV/f.u., Curie temperature $T_c > 800$ K determined by the mean-field approach, and magnetization $\mu_0 M_s > 1$ T are discussed.

Keywords: ab initio calculations; magnetocrystalline anisotropy; magnetization; rare-earth-free magnets

1. Introduction

Magnetic materials are crucial for technological development in many sectors, such as electric motors, transformers, power generators, and recording media. High-performance permanent magnets with a large saturation magnetization, high Curie temperature, and large uniaxial magnetic anisotropy are necessary, with these requirements currently being fulfilled by rare-earth permanent magnets such as Sm–Co and Nd–Fe–B [1]. The volatile prices and restricted accessibility to rare-earth resources raised a strategic issue, directing the research efforts in the last two decades to the search for new magnetic materials with close performance to Sm–Co and Nd–Fe–B magnets but with lower rare-earth content. Also, the search for new permanent magnets without rare-earth elements has aroused research interest in magnetic materials [2–4]. Due to their reduced costs and small supply risks, their use in less demanding applications can be efficient. This research direction is motivated by the large gap in the price–performance diagram between the hard ferrite/alnico magnets and the high-performance RE, which could be filled by new rare-earth-free permanent magnets. In this last category, the Fe compounds with an anisotropic crystal structure are important candidates for functional rare-earth-free permanent magnets due to their lower price, standardized preparation procedure, and good mechanical properties. One such compound is Fe$_5$SiB$_2$, discovered in the 1960s by Aronsson et al. [5], which crystallizes in the Cr$_5$B$_3$ structure type (*I4/mcm* space group). According to recent research, a saturation magnetization $M_s = 9.2$ μ_B/f.u. (1.34 MA/m) was theoretically predicted for this compound [6]. The magnetic measurements at 10 K show a considerably lower value of M_s of 1.1 MA/m, while large values of spin magnetic moments on both Fe crystal sites (2.31 μ_B

for Fe on the *4c* site and 2.10 μ_B for Fe on the *16l* site) were determined by neutron diffraction at 16 K [7]. Several investigations reported Curie temperatures over 800 K for this compound [7,8]. Also, a magnetic anisotropy constant $|K_1|$ of 0.25 MJ/m^3 was estimated from the $1/H^2$ term of magnetization *M* vs. magnetic field *H* dependence [6]. The spin orientation was revealed by the Mössbauer spectroscopy of Ericsson et al. [9] and the neutron diffraction experiments of Cedervall et al. [7]. The Fe$_5$SiB$_2$ alloy is a simple ferromagnet with in-plane spins at low temperatures and spins parallel to the c-axis for temperatures between ~140 K and the Curie temperature [9]. Despite the large values of saturation magnetization and Curie temperature of the Fe$_5$SiB$_2$ alloy, due to its in-plane anisotropy and spin reorientation [7], this compound is considered inefficient for the development of permanent magnets (PMs). Further research found that the Co for Fe substitution in (Fe,Co)$_5$SiB$_2$ can turn the sign of MAE from negative to positive, enabling an axial easy magnetization direction for the corresponding alloys. Also, the spin-reorientation transition temperature is decreased by Co-doping to the lowest temperature [10]. Other studies report a moderate improvement of magnetic anisotropy by Ge and P for Si substitutions in the Fe$_5$SiB$_2$ alloy, respectively [11–13], along with the decrease in the spin-reorientation temperature to 60 K [11] and 10 K [13].

On the other hand, previous studies showed that doping with *5d* elements (M) builds stronger uniaxial anisotropy in Fe alloys, due to the stronger spin–orbit coupling of Fe–*3d* and M–*5d* states [14,15]. The earlier research of Thakur et al. on Fe$_5$PB$_2$ doped with W [16] showed that the anisotropy constant K_1 increases from 0.152 MJ/m^3 in Fe$_5$PB$_2$ to 1.135 MJ/m^3 in Fe$_4$WPB$_2$, and this enhancement is attributed to the strong spin–orbit coupling of Fe–*3d* states and W–*5d* states. Still, the magnetization and the Curie temperature are decreased by *5d*-doping in Fe alloys, substituting Fe with a nonmagnetic element. In this case, the doping amount has to be optimized to keep the intrinsic magnetic properties at values compatible with functional applications. Our previous theoretical investigations showed for the Fe$_4$WSiB$_2$ alloy an anisotropy constant of 0.218 meV/f.u. In this case, W-doping in Fe$_5$SiB$_2$ improves the anisotropy at the cost of the magnetization reduction (to 7.97 μ_B/f.u.) and the Curie temperature decrease (747 K) [17].

Also, other *5d* elements could be effective for magnetic anisotropy tailoring. For instance, *5d*-doping in an Fe$_2$B alloy showed larger efficiency for Re-doping (K_1 = 1.5 MJ/m^3, magnetization $\mu_0 M_s$ = 1.22 T and an estimated Curie temperature of 595 K for Fe$_{1.52}$Re$_{0.48}$B), whilst the W-doping effects on anisotropy are much weaker [18].

In this study, we present the magnetic anisotropy behavior of *5d*-doping in Fe$_{5-x-y}$Co$_x$M$_y$SiB$_2$ alloys (M = W and Re) in the range $0 \leq x \leq 2$ and $0 \leq y \leq 1$. The Co- and M-doping ranges were chosen accounting for the substitution effects on MAE, Curie temperatures, and magnetization in (Fe,Co)$_5$SiB$_2$ alloys. The balance between the benefit of doping for the anisotropy and its detrimental influence on the magnetization and Curie temperature restricted the x and y choice. The Co-doping needed to change the sign of MAE (x > 1) was reported, while for x > 2, the Curie temperatures T$_c$ of the (Fe,Co)$_5$SiB$_2$ alloys are less appropriate for permanent magnet applications (T$_c$ < 500 K) [6,8]. A similar expected decrease in magnetization and Curie temperatures by a nonmagnetic *5d* element, M, for Fe substitution limits the y-doping in our study to y = 1.
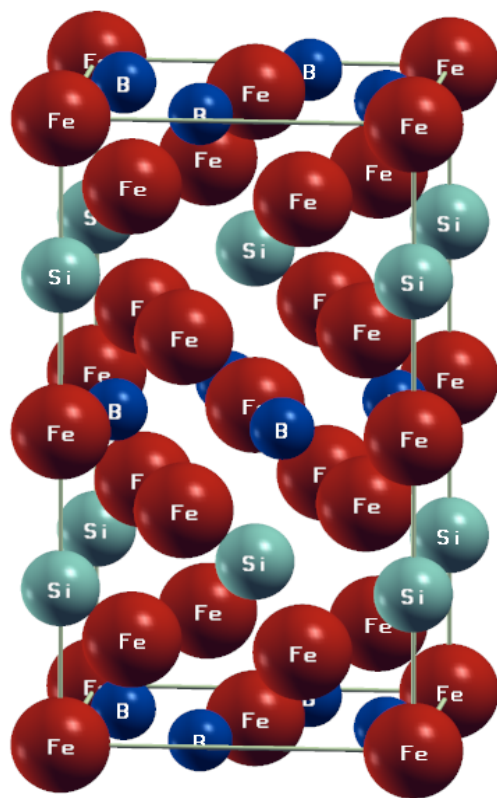
Two-dimensional maps of the anisotropy constant were built, allowing for the selection of the composition range for compounds with large uniaxial anisotropies. Further investigations on the magnetization and Curie temperature behavior vs. Co and M content (M = W and Re) enable a detailed view of the intrinsic magnetic properties of these alloys. Fully relativistic theoretical calculations in the framework of density functional theory (DFT) using the exchange–correlation potential under general gradient approximation were employed for the current investigations. The torque method for magnetic anisotropy energy calculations was used. The Curie temperatures were evaluated using the Heisenberg exchange interaction parameters extracted from DFT results and used as inputs for the mean field approach calculations.

2. Results and Discussion

2.1. Crystal Structure

The crystal structure of the $Fe_{5-x-y}Co_xM_ySiB_2$ alloys (Figure 1) consists of a body-centered tetragonal unit cell (space group *I4/mcm*, no. 140), with Fe atoms on two different sites (*4c* and *16l*) and B atoms on 8h sites, whilst Si atoms occupy the 4a crystallographic sites. The lattice parameters determined by X-ray diffraction are a = 5.5541 Å and c = 10.3429 Å [7].

Electronic band-structure calculations for the $Fe_{5-x-y}Co_xM_ySiB_2$ alloys (for $0 \leq x \leq 2$ and $0 \leq y \leq 1$) in the tetragonal structure (space group *I4/mcm*) using the experimental lattice parameters [2,19] were performed. The experimental free parameters of *8h* and *16l* crystallographic sites, determined by Cedervall et al. for Fe_5SiB_2, were considered [7]. The lattice constants of the W- and Re-doped alloys were evaluated using the lattice constants of Re_5SiB_2, W_5SiB_2, and Co_5SiB_2 [7,19], considering their linear dependence via doping. The low effect of the structural relaxation on MAE in Fe compounds evidenced by Lawrence et al. [20], as well as the low effect of pressure on the magnetization and Curie temperature of Fe_5SiB_2 [21], allowed us to rely on this estimated lattice constants. The occupation of Co atoms on *16l* crystal sites was considered, according to our previous investigations [8]. A similar preferential occupation was obtained for Re atoms, whilst a random occupation of the *4c* and *16l* sites was derived for W atoms by total energy calculations.

Figure 1. The body-centered tetragonal unit cell (space group *I4/mcm*, no. 140) of Fe_5SiB_2 alloy, with Fe atoms on two different sites (*4c* and *16l*), the B atoms on 8h sites, and Si atoms on 4a crystallographic sites. The graphic program XCrySDen [22] was used.

2.2. Magnetic Moments

Band-structure calculations for the Fe_5SiB_2 alloy were performed using different exchange and correlation parametrizations (local density approximation (LDA) and general gradient approximation (GGA)) with atomic sphere approximation as well as the full-potential approach. The results of the calculations are listed in Table 1, together with

the results of experimental measurements [7] and other theoretical results based on the full-potential local orbital minimum-basis method (FPLO) [6].

Table 1. Total magnetic moments and site-dependent spin and orbital magnetic moments for the Fe_5SiB_2 alloy, determined by different exchange–correlation approaches in the ASA and full-potential mode. Present calculations based on the spin-polarized relativistic Korringa–Kohn–Rostoker method (SPR-KKR) [23] (details in Section 3) are compared with theoretical full-potential local orbital minimum-basis method (FPLO) results [6]. The experimental values for saturation magnetization and neutron diffraction [6,7] are also shown.

	SPR-KKR						FPLO [6]		Neutron Diffraction [7]
	VWN-ASA		GGA-ASA		GGA-FP		GGA-FP		
	m_s (μ_B)	m_l (μ_B)	m_s (μ_B)	m_l (μ_B)	m_s (μ_B)	m_l (μ_B)	m_s (μ_B)	m_l (μ_B)	m_{tot} (μ_B)
Fe *4c*	2.20	0.05	2.35	0.05	2.08	0.05	2.24	0.05	2.31
Fe *16l*	1.61	0.04	1.81	0.04	1.88	0.04	1.87	0.04	2.10
Si *4a*	−0.14	-	−0.17	-	−0.16	-	−0.25	-	-
B *8h*	−0.13	-	−0.15	-	−0.14	-	−0.25	-	-
Total (μ_B/f.u.)	8.25	0.21	9.12	0.22	9.19	0.22	8.98	0.22	10.71
	8.46		9.34		9.41		9.20		
Exp. M_s(μ_B/f.u.) [7]					9.35				

According to our calculations, the Fe_5SiB_2 alloy is ferromagnetic, with a total magnetic moment between 8.46 and 9.41 μ_B/f.u., depending significantly on the exchange–correlation potential and the potential symmetry (spherical in ASA and no shape approximation in the full-potential approach). As can be seen in Table 1, the VWN-ASA approach gives an underestimated total magnetic moment compared with the experimental data. Better agreement is obtained by the use of the GGA approach, with a total magnetic moment of 9.34 μ_B/f.u. (GGA-ASA) and 9.41 μ_B/f.u. (GGA-FP). Also, the SPR-KKR shows similar values of individual magnetic moments with FPLO calculations with only minor deviations, determined most probably by the lattice constants used for calculations. The Fe magnetic moments show higher values for Fe *4c*, but the ratio between Fe *4c/16l* moments depends on the calculation approach.
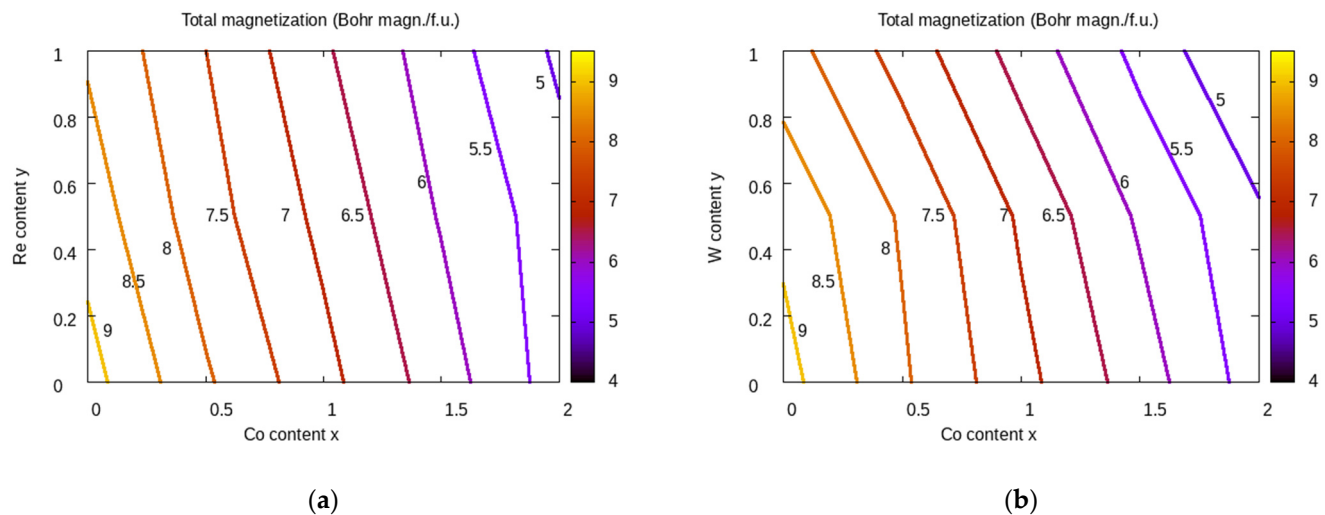
Based on these results, the GGA-ASA calculation mode was chosen to deal with the combined Co- and M (M = Re, W)-doping. Moreover, the GGA-ASA calculated value of $\mu_0 M_s$ (1.36 T) is close to the value determined experimentally by McGuire et al. (1.31 T) [10].

The total magnetic moments calculated for the $Fe_{5−x−y}Co_xM_ySiB_2$ alloys for $0 \leq x \leq 2$ and $0 \leq y \leq 1$ were used to build a two-dimensional map of magnetization vs. Co and M content (x,y), shown in Figure 2. According to the contour maps for several selected values of total magnetic moment, the Re- and W-doping have a similar effect in combination with Co-doping on the magnetization of the $Fe_{5−x−y}Co_xM_ySiB_2$ alloys. The values of magnetization are decreased by both combined doping types (Co and Re; Co and W, respectively) from 9.34 μ_B/f.u. to values lower than 5 μ_B/f.u. The decrease in magnetization has already been evidenced for doping with Co [6,8]. Still, the use of combined doping (Co + Re; Co + W) can enhance this tendency, as shown in Figure 2. If the desired values of magnetization are set to values over 6 μ_B/f.u., the corresponding alloys have Co content $x \leq 1.5$ and M content $y \leq 0.6$.
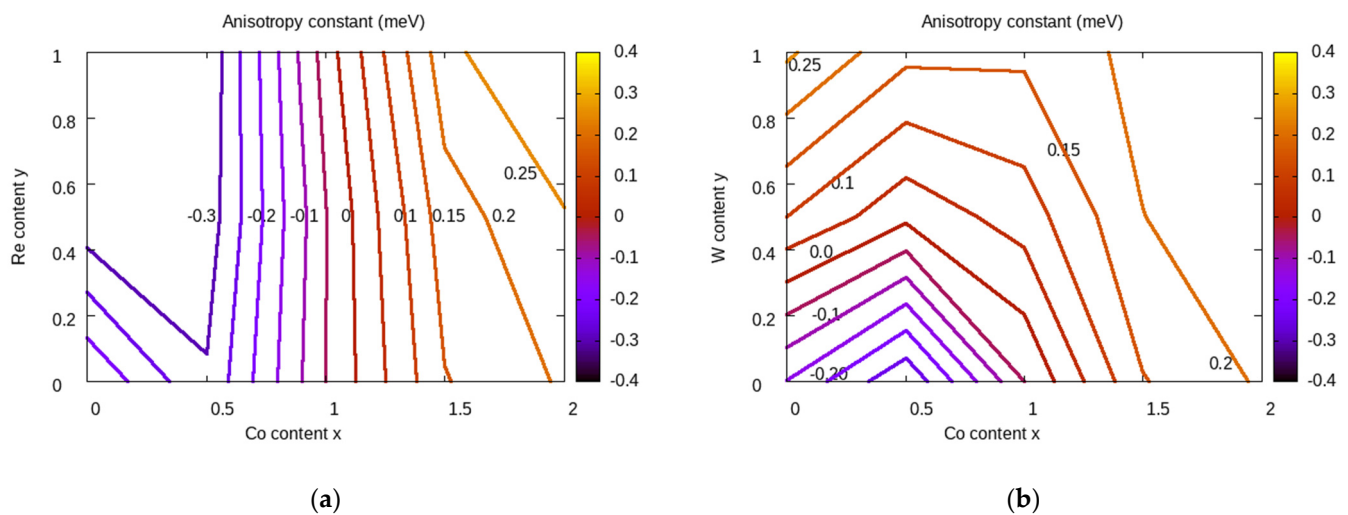
2.3. Magnetic Anisotropy

The earlier reports show that the anisotropy constant of $(Fe,Co)_5SiB_2$ alloys changes the sign for a certain range of Co amount [6,8]. This effect is accounted for in the present study, as easy-axis anisotropy is obtained by Co-doping, followed by expected anisotropy enhancement by further doping with *5d* elements. The validity of this mechanism is discussed below, using the representation of the anisotropy constants K_1 calculated for $Fe_{5−x−y}Co_xM_ySiB_2$ alloys. The K_1 values obtained for both M = Re and W in a 5×3 grid

for $0 \leq x \leq 2$ and $0 \leq y \leq 1$ ($\Delta x = \Delta y = 0.5$) were used to build the $K_1(x,y)$ 2D maps. The K_1 isolines between -0.3 meV/f.u and 0.25 meV/f.u. are shown in Figure 3. As can be seen, significantly different K_1 2D maps were obtained by Re-/W-doping in $Fe_{5-x-y}Co_xM_ySiB_2$ alloys. In the case of Re, values of K_1 over 0.25 meV/f.u. can be obtained for a combination of Co-doping with approx. $x \geq 1.8$ and Re-doping with $y \geq 0.7$. The disadvantage of the Re-doping is made visible by overlapping the M_s 2D map (Figure 2) and K_1 2D map (Figure 3). The (x,y) areas with large K_1 values almost overlap with the areas with low magnetization values, as $M_s < 5$ μ_B/f.u. for $x \geq 1.5$. This behavior of magnetocrystalline anisotropy is opposite to that evidenced in the Fe_2B alloy, where Re-doping promoted large axial anisotropy [18].

(**a**)　　　　　　　　　　　　　　　　　　　(**b**)

Figure 2. The calculated total magnetization for the $Fe_{5-x-y}Co_xM_ySiB_2$ alloys for M = Re (**a**) and M = W (**b**) is represented as 2D maps of Co vs. M content (x, y). The isolines for discrete values of magnetization (in μ_B/f.u.) are shown. The preferential occupation by Co+M-doping was accounted for in the total energy calculations (Co and Re on *16l* site, random occupation on *4c* and *16l* sites for W).

(**a**)　　　　　　　　　　　　　　　　　　　(**b**)

Figure 3. The calculated anisotropy constants for the $Fe_{5-x-y}Co_xM_ySiB_2$ alloys for (**a**) M = Re and (**b**) M = W are represented as 2D maps of Co vs. M content (x, y). The isolines for discrete values of K_1 (in meV) are shown. The preferential occupation by Co+M-doping was accounted for in the total energy calculations (Co and Re on *16l* site, random occupation on *4c* and *16l* sites for W).
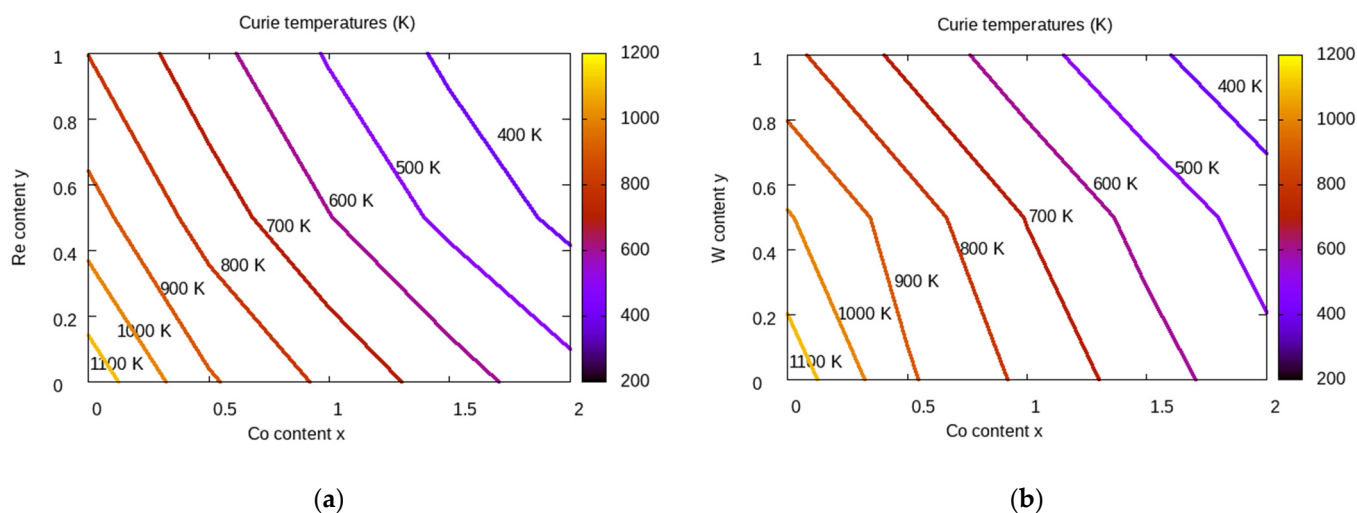
On the other hand, W-doping can increase the anisotropy of the Fe_5SiB_2 alloy, with values of $K_1 \geq 0.2$ meV/f.u. being obtained for x = 0 and y > 0.8. Also, values of $K_1 \geq 0.25$ meV/f.u. are seen for x = 0 and y~1. By overlapping the 2D maps of M_s and K_1 in the case of M = W, one can find magnetization values between 8 and 8.5 μ_B/f.u. It is interesting to note that in the case of Re-doping, the area (x = 0, y > 0.9) corresponds to the largest value of in-plane magnetocrystalline anisotropy, whilst W-doping alone can switch the anisotropy to easy-axis anisotropy without additional Co-doping.

2.4. Curie Temperatures and Exchange-Coupling Parameters

The Curie temperatures (T_c) were determined by the mean field approach (MFA) using the procedure described in Section 3. The grid data for T_c were used to build isolines with constant values of T_c, which are represented in Figure 4. According to our calculations, the Fe_5SiB_2 alloy is ferromagnetic with a Curie temperature of 1162 K, calculated with the mean field approach. As the mean field method is known to overestimate the Curie temperature values by ~20%, the estimated T_c would be comparable with the experimental value of 850 K [8].

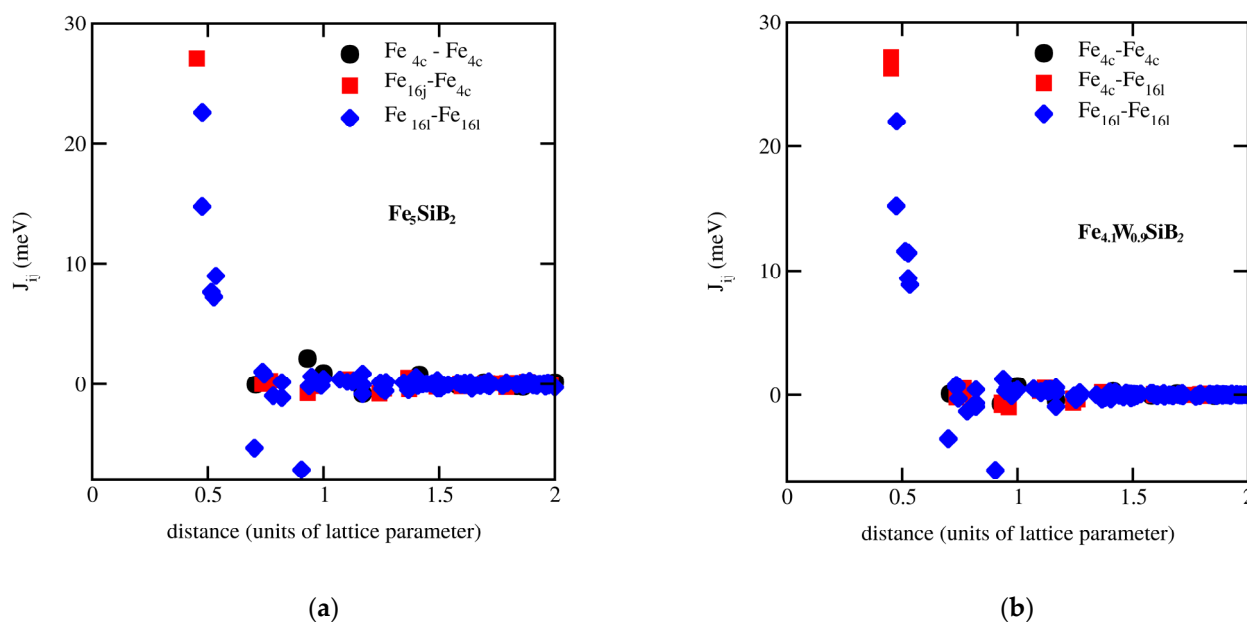**Figure 4.** The calculated Curie temperatures for the $Fe_{5-x-y}Co_xM_ySiB_2$ alloys for (**a**) M = Re and (**b**) M = W are represented as 2D maps of Co vs. M content (x, y). The isolines for discrete values of T_c (in K) are shown. The preferential occupation by Co+M-doping was accounted for in the total energy calculations (Co and Re on *16l* site, random occupation on *4c* and *16l* sites for W).

From the T_c representation in Figure 4, it is obvious that the combined Co + M-doping will decrease the Curie temperatures for both M = Re and W. This decrease is slightly steeper in the case of Co + Re. For Re-doped alloys, by overlapping the areas where $K_1 \geq 0.2$ meV/f.u. on the K_1 2D map with the Curie temperature map, the corresponding alloys have T_c values under 400 K, which makes the Re-doping rather unsuitable for PM applications.

On the other hand, the expected T_c values of the W-doped alloys with anisotropy constant $K_1 \geq 0.2$ meV/f.u. (obtained for x = 0 and y > 0.8) are between 850 and 900 K, compatible with PM applications.

Due to the promising intrinsic properties of $Fe_{1-y}W_ySiB_2$ alloys in the doping range y > 0.8, we investigated in more detail the magnetic properties of such W-doped alloys. We used a complementary approach by considering particular microscopic models, making use of magnetic interaction based on the classical Heisenberg Hamiltonian described in Section 3. Using this approach, the Fe–Fe exchange-coupling parameters are obtained and represented as a function of distance (in units of lattice constant a). The Fe–Fe exchange interactions for Fe_5SiB_2 and $Fe_{4.1}W_{0.9}SiB_2$ alloys are presented in Figure 5. As can be seen in Figure 5, the dominant exchange interactions are positive, favoring ferromagnetic ordering.

Negative exchange interactions are also seen, mostly between Fe *16l* spins at distances of between 0.6a and 0.9a. The largest exchange interactions are between Fe *4c*–Fe *16l* nearest neighbors. These exchange interactions are affected by the W-doping, and a decrease in the exchange-coupling parameters between nearest neighbors in $Fe_{4.1}W_{0.9}SiB_2$ compared with Fe_5SiB_2 can be seen. Also, a decrease in the exchange-coupling parameter values by W-doping is observed for the interactions between the Fe *4c*–Fe *4c* spins. The exchange interactions between nearest Fe *4c*–Fe *4c* spins are much smaller, as their interatomic distance is considerably larger than those of the other pairs. The Curie temperature is mostly determined by the Fe *16l*–Fe *16l* and Fe *4c*–Fe *16l* exchange interactions.

(**a**)   (**b**)

Figure 5. The Fe–Fe exchange-coupling parameters for (**a**) Fe_5SiB_2 and (**b**) $Fe_{4.1}W_{0.9}SiB_2$ alloys plotted as a function of the distance between Fe spins. The preferential occupation by W-doping was accounted for in the total energy calculations (random occupation on *4c* and *16l* sites for W).

The spin and orbital magnetic moments, magnetization $\mu_0 M_s$, anisotropy constant K_1, Curie temperature, and hardness parameter for the $Fe_{4.1}W_{0.9}SiB_2$ alloy are listed in Table 2. In particular, the spin and orbital moments on Fe sites (2.43 μ_B and 0.07 μ_B for Fe *4c*; 1.95 μ_B and 0.06 μ_B for Fe *16l*) are higher compared with the corresponding values in Fe_5SiB_2 (see Table 1), but the weight of the magnetic atoms decreases by about 18%, resulting in a magnetization decrease (8.37 μ_B/f.u.) by W-doping, which corresponds to a $\mu_0 M_s$ value of 1.17 T.

Table 2. Spin and orbital magnetic moments and magnetization $\mu_0 M_s$, together with the magnetocrystalline anisotropy constant K_1 and Curie temperature for the $Fe_{4.1}W_{0.9}SiB_2$ alloy.

	Lattice Const. a,c (Å)	m_s (μ_B/f.u.)	m_l (μ_B/f.u.)	$\mu_0 M_s$ (T)	K_1 (meV/f.u.)	K_1 (MJ/m³)	κ	T_c (K)
$Fe_{4.1}W_{0.9}SiB_2$	5.64; 10.47	8.14	0.23	1.17	0.24	0.46	0.65	863

The results from Table 2 show that $Fe_{4.1}W_{0.9}SiB_2$ alloy is a semi-hard permanent magnet, with $\mu_0 M_s > 1$T and a magnetic anisotropy energy of 0.46 MJ/m³, close to the values in Sr ferrite [4]. The magnetic hardness parameter captures the potential of the present alloy, with adequate magnetization $\mu_0 M_s$ (1.17 T), to be developed into a compact permanent magnet. The value obtained according to the formula $\kappa = \sqrt{K_1/\mu_0 M_s^2}$ is 0.65, corresponding to a semi-hard magnetic material. The Curie temperature is expected to be overestimated by MFA, but a value over 680 K is still expected for the $Fe_{4.1}W_{0.9}SiB_2$ alloy.

The high value of the Curie temperature allows for the use of these alloys in relatively high-temperature applications.

3. Materials and Methods

Spin-polarized fully relativistic band-structure calculations based on the Korringa–Kohn–Rostoker (SPRKKR) method were used for theoretical calculations [23]. This calculation method is based on the KKR–Green function formalism that makes use of the multiple scattering theory. Within this approach, the so-called t-scattering matrices describing the scattering properties of each scattering center (atom) are determined. In the second step, the multiple scattering matrices of all atoms in the lattice are calculated accounting for the fact that the incident wave at each atom is the sum of the outgoing waves from all other atoms. The central role in the KKR–Green function method is played by the crystal Green's function, which is efficiently related to Green's function of free space via the Dyson equation. The SPR-KKR calculation method supplies all the information about the electronic structure, similar to other band-structure methods that use energy eigenvalues and eigenfunctions to represent the electronic structure. In addition, the SPR-KKR band-structure method has an important advantage in dealing with chemical disorder, as the coherent potential approximation (CPA) [24] was efficiently integrated by defining Green's function of the average crystal medium, which is determined self-consistently through the condition that the concentration average of the various atom types should not produce any additional scattering in this medium [24]. In this way, the SPR-KKR is a more efficient and reliable alternative to more laborious supercell techniques, requiring enlarged unit cells and atomic-configuration averaging in the supercells to describe the alloy's properties. The 7.7 version of the Munich SPR-KKR band-structure program was used for the present investigations [25]. More details about the SPR-KKR method are extensively described elsewhere [23,25].

Local spin-density approximation (LSDA) [26] and generalized gradient approximation with the parametrization of Perdew et al. (GGA-PBE) [27] were used to account for the exchange and correlation effects. The k-space integration was performed using the special points method [28]. The study of magnetic anisotropy was performed with magnetic torque calculations. The magnetic torque acting on the magnetic moment $\vec{m}_i$ of the atomic site *I*, oriented along the magnetization direction $\vec{M}$, generates a component:

$$T_{\hat{u}}(\theta, \varphi) = -\partial E(\vec{M}(\theta, \varphi))/\partial \theta \tag{1}$$

with respect to the axis $\hat{u}$, where θ and φ are the polar angles [29,30]. The magnetic anisotropy energy, defined as the energy difference between the in-plane and out-of-plane magnetization directions, is related to the magnetic torque by a special geometry. By setting the polar angles to $\theta = \pi/4$ and $\varphi = 0$, the calculated magnetic torque is $T_{\hat{u}}(\pi/4, 0) = E_{[100]} - E_{[001]}$ [30]. The total energy for the tetragonal symmetry by first-order approximation of the magnetic anisotropy energy is given by the expression $E_a = K_1 sin^2\theta + K_2 sin^4\theta$, where K_1 and K_2 are the anisotropic constants and θ is the polar angle between the magnetization direction and the easy axis. In the case of the Fe_5SiB_2 alloy, $K_2 \ll K_1$ [7,13], and the magnetic anisotropy energy is described by K_1. The easy-plane anisotropy corresponds to negative values of K_1. A dense k-mesh of $25 \times 25 \times 25$ k-points in the Brillouin zone was used for magnetic torque calculations.

The magnetic behavior of $Fe_{5-x-y}Co_xM_ySiB_2$ alloys was investigated using a complementary approach based on the classical Heisenberg Hamiltonian described by the expression:

$$H_{ex} = -\sum_{i,j} J_{ij} \hat{e}_i \cdot \hat{e}_j \tag{2}$$

where the summation is performed on all lattice sites *i* and *j*, and $\hat{e}_i$ and $\hat{e}_j$ are the unit vectors of magnetic moments on sites *i* and *j*, respectively. The total energy difference

ΔE_{ij} due to an infinitesimal change in angle between the magnetic moments of the (i, j) spin pair was calculated in scalar-relativistic mode and expressed to the lowest order with respect to the orientation angle between $\hat{e}_i$ and $\hat{e}_j$. Using the expression derived by Liechtenstein [29] based on the magnetic force theorem, a one-to-one mapping between the exchange-coupling energy ΔE_{ij} and the Heisenberg Hamiltonian is obtained, allowing for the determination of the J_{ij} exchange-coupling parameters. The J_{ij} exchange-coupling parameters were calculated for all magnetic atoms as a function of distance up to 15 Å around each lattice site. The mean field approach (MFA) was used to derive the Curie temperatures using the calculated J_{ij} exchange-coupling parameters, according to the expression [29,31]:

$$T_c^{MFA} = \frac{2}{3k_B} \sum_i J_{0i} \tag{3}$$

where J_{0i} is the exchange-coupling parameter on ith site, and the sum runs over all coordination shells.

4. Conclusions

The aim of the present research was to identify the M $5d$-doping elements and the doping amount able to switch to easy-axis anisotropy and enhance it by enabling strong spin–orbit coupling between the Fe–$3d$ and M–$5d$ states. Theoretical studies on the $Fe_{5-x-y}Co_yW_xSiB_2$ alloys show a decrease in the total magnetic moment and Curie temperatures of the alloys by increasing W and Re content x. Also, the theoretically calculated anisotropy constant turns from planar for the Fe_5SiB_2 alloy to axial for $Fe_{5-x-y}Co_yW_xSiB_2$ in different zones of the 2D map, showing the opposite impact of Re-/W-doping on the magnetocrystalline anisotropy behavior in these alloys. The superposition of the 2D maps for magnetization, MAE, and Curie temperatures allowed us to conclude that W-doping is favorable for the development of intrinsic properties compatible with PM applications, even without Co-doping. In the case of Re + Co-doping, such a concentration range was not found due to the reversed effects of combined doping on the magnetization and Curie temperature on one side and magnetocrystalline anisotropy on the other side. Despite its strong spin–orbit coupling with Fe–$3d$ states, Re-doping determined large anisotropy constants for the alloys with low Curie temperatures and magnetizations, incompatible with PM applications. On the other hand, the W-doped Fe_5SiB_2 alloys can be optimized to allow for their use as semi-hard magnets in nanocomposite magnetic materials.

Conflicts of Interest: The author declare no conflict of interest. The funders had no role in the design of the study; in the collection, analyses, or interpretation of data; in the writing of the manuscript; or in the decision to publish the results.

References

1. Coey, J.M.D. Perspective and Prospects for Rare Earth Permanent Magnets. *Engineering* **2020**, *6*, 119–131. [CrossRef]
2. Mohapatra, J.; Liu, J.P. Rare-Earth-Free Permanent Magnets: The Past and Future. In *Handbook of Magnetic Materials*; Elsevier: Amsterdam, The Netherlands, 2018; Volume 27, pp. 1–57. [CrossRef]
3. Skokov, K.P.; Gutfleisch, O. Heavy rare earth free, free rare earth and rare earth free magnets—Vision and reality. *Scr. Mater.* **2018**, *154*, 289–294. [CrossRef]
4. Cui, J.; Kramer, M.; Zhou, L.; Liu, F.; Gabay, A.; Hadjipanayis, G.; Sellmyer, D. Current progress and future challenges in rare-earth-free permanent magnets. *Acta Mater.* **2018**, *158*, 118–137. [CrossRef]
5. Aronsson, B.; Engström, I. X-ray Investigations on Me-Si-B Systems (Me = Mn, Fe, Co). *Acta Chem. Scand* **1960**, *14*, 1403. [CrossRef]
6. Werwiński, M.; Kontos, S.; Gunnarsson, K.; Svedlindh, P.; Cedervall, J.; Höglin, V.; Sahlberg, M.; Edström, A.; Eriksson, O.; Rusz, J. Magnetic properties of Fe_5SiB_2 and its alloys with P, S, and Co. *Phys. Rev. B* **2016**, *93*, 174412. [CrossRef]
7. Cedervall, J.; Kontos, S.; Hansen, T.C.; Balmes, O.; Martinez-Casado, F.J.; Matej, Z.; Beran, P.; Svedlindh, P.; Gunnarsson, K.; Sahlberg, M. Magnetostructural transition in Fe_5SiB_2 observed with neutron diffraction. *J. Solid State Chem.* **2016**, *235*, 113–118. [CrossRef]

8. Hirian, R.; Isnard, O.; Pop, V.; Benea, D. Investigations on the magnetic properties of the $Fe_{5-x}Co_xSiB_2$ alloys by experimental and band structure calculation methods. *J. Magn. Magn. Mater.* **2020**, *505*, 166748. [CrossRef]

9. Ericsson, T.; Häggström, L.; Wäppling, R. Spin rotation in Fe_5SiB_2. *Phys. Scr.* **1978**, *17*, 83–86. [CrossRef]

10. McGuire, M.A.; Parker, D.S. Magnetic and structural properties of ferromagnetic Fe_5PB_2 and Fe_5SiB_2 and effects of Co and Mn substitutions. *J. Appl. Phys.* **2015**, *118*, 163903. [CrossRef]

11. Lejeune, B.T.; Barua, R.; McDonald, I.J.; Gabay, A.M.; Lewis, L.H.; Hadjipanayis, G.C. Synthesis and processing effects on magnetic properties in the Fe_5SiB_2 system. *J. Alloys Compd.* **2018**, *731*, 995–1000. [CrossRef]

12. Clulow, R.; Hedlund, D.; Vishina, A.; Svedlindh, P.; Sahlberg, M. Magnetic and structural properties of the $Fe_5Si_{1-x}GexB_2$ system. *J. Solid State Chem.* **2022**, *316*, 123576. [CrossRef]

13. Hedlund, D.; Cedervall, J.; Edström, A.; Werwiński, M.; Kontos, S.; Eriksson, O.; Rusz, J.; Svedlindh, P.; Sahlberg, M.; Gunnarsson, K.J. Magnetic properties of the $Fe_5SiB_2-Fe_5PB_2$ system. *Phys. Rev. B* **2017**, *96*, 094433. [CrossRef]

14. Edström, A.; Werwiński, M.; Rusz, J.; Eriksson, O.; Skokov, K.P.; Radulov, I.A.; Ener, S.; Kuz'min, M.D.; Hong, J.; Fries, M.; et al. Effect of doping by 5d elements on magnetic properties of alloys, Magnetic properties of $(Fe_{1-x}Co_x)_2B$ alloys and the effect of doping by 5d elements. *Phys. Rev. B* **2015**, *92*, 174413. [CrossRef]

15. Khan, I.; Hong, J. Site dependent enhancement of magnetic anisotropy in 4d and 5d impurity doped α-$Fe_{16}N_2$: A first principles study. *Curr. Appl. Phys.* **2018**, *18*, 526–533. [CrossRef]

16. Thakur, J.; Rani, P.; Tomar, M.; Gupta, V.; Kashyap, M.K. Enhancement of magnetic anisotropy of Fe_5PB_2 with W substitution: Ab-initio study. *AIP Conf. Proc.* **2019**, *2093*, 020012. [CrossRef]

17. Hirian, R.; Pop, V.; Isnard, O.; Benea, D. Magnetic properties of the $(Fe,Co)_5SiB_2$ alloys by W doping. *Stud. UBB Phys.* **2022**, *67*, 1. [CrossRef]

18. Benea, D.; Pop, V. Magnetic Properties of the Fe_2B Alloy Doped with Transition Metal Elements. *Magnetochemistry* **2023**, *9*, 109. [CrossRef]

19. Lawrence, R.A.; Donaldson, S.J.; Probert, M.I. Magnetic Transition State Searching: Beyond the Static Ion Approximation. *Magnetochemistry* **2023**, *9*, 42. [CrossRef]

20. Kaštil, J.; Hirian, R.; Isnard, O. Effect of pressure on the magnetic and structural properties of Fe_5SiB_2 compound. *Intermetallics* **2019**, *110*, 106484. [CrossRef]

21. Pan, Y.; Guan, W.M. Exploring the structural stability and mechanical properties of TM_5SiB_2 ternary silicides. *Ceram. Int.* **2018**, *44*, 9893. [CrossRef]

22. Kokalj, A. XCrySDen—A new program for displaying crystalline structures and electron densities. *J. Mol. Graph. Model.* **1999**, *17*, 176–179. [CrossRef] [PubMed]

23. Ebert, H.; Ködderitzsch, D.; Minar, J. Calculating condensed matter properties using the KKR-Green's function method—Recent developments and applications. *Rep. Prog. Phys.* **2011**, *74*, 096501. [CrossRef]

24. Faulkner, J.S.; Stocks, G.M. Calculating properties with the coherent-potential approximation. *Phys. Rev. B* **1980**, *21*, 3222. [CrossRef]

25. Munich SPRKKR Band Structure Program Package. Available online: https://www.ebert.cup.uni-muenchen.de/index.php/de/software/13-sprkkr (accessed on 8 December 2023).

26. Vosko, S.H.; Wilk, L.; Nusair, M. Accurate spin-dependent electron liquid correlation energies for local spin density calculations: A critical analysis. *Can. J. Phys.* **1980**, *58*, 1200. [CrossRef]

27. Perdew, J.P.; Burke, K.; Ernzerhof, M. Generalized Gradient Approximation Made Simple. *Phys. Rev. Lett.* **1996**, *77*, 3865. [CrossRef] [PubMed]

28. Monkhorst, H.; Pack, J. Special points for Brillouin-zone integrations. *Phys. Rev. B* **1976**, *13*, 5188. [CrossRef]

29. Liechtenstein, A.I.; Katsnelson, M.I.; Antropov, V.P.; Gubanov, V.A. Local spin density functional approach to the theory of exchange interactions in ferromagnetic metals and alloys. *J. Magn. Magn. Mater.* **1987**, *67*, 65–74. [CrossRef]

30. Mankovsky, S.; Polesya, S.; Minar, J.; Hoffmann, F.; Back, D.H.; Ebert, H. Spin-orbit coupling effect in (Ga, Mn) As films: Anisotropic exchange interactions and magnetocrystalline anisotropy. *Phys. Rev. B* **2011**, *84*, 201201. [CrossRef]

31. Nieves, P.; Arapan, S.; Maudes-Raedo, J.; Marticorena-Sánchez, R.; Del Brío, N.L.; Kovacs, A.; Echevarria-Bonet, C.; Salazar, D.; Weischenberg, J.; Zhang, H.; et al. Database of novel magnetic materials for high-performance permanent magnet development. *Comput. Mat. Sci.* **2019**, *168*, 188–202. [CrossRef]